Mercury Speciation by X-ray Absorption Fine Structure Spectroscopy and Sequential Chemical Extractions: A Comparison of Speciation Methods

CHRISTOPHER S. KIM,*,†
NICOLAS S. BLOOM,‡
JAMES J. RYTUBA,§ AND
GORDON E. BROWN, JR.†,‖

Surface and Aqueous Geochemistry Group, Department of Geological and Environmental Sciences, Stanford University, Stanford, California 94305-2115, Frontier Geosciences, 414 Pontius North, Seattle, Washington 98109, U.S. Geological Survey, 345 Middlefield Road, MS 901, Menlo Park, California 94025, and Stanford Synchrotron Radiation Laboratory, SLAC, 2575 Sand Hill Road, MS 99, Menlo Park, California 94025

Determining the chemical speciation of mercury in contaminated mining and industrial environments is essential for predicting its solubility, transport behavior, and potential bioavailability as well as for designing effective remediation strategies. In this study, two techniques for determining Hg speciation—X-ray absorption fine structure (XAFS) spectroscopy and sequential chemical extractions (SCE)—are independently applied to a set of samples with Hg concentrations ranging from 132 to 7539 mg/kg to determine if the two techniques provide comparable Hg speciation results. Generally, the proportions of insoluble HgS (cinnabar, metacinnabar) and HgSe identified by XAFS correlate well with the proportion of Hg removed in the aqua regia extraction demonstrated to remove HgS and HgSe. Statistically significant ($>$10%) differences are observed however in samples containing more soluble Hg-containing phases ($HgCl_2$, HgO, $Hg_3S_2O_4$). Such differences may be related to matrix, particle size, or crystallinity effects, which could affect the apparent solubility of Hg phases present. In more highly concentrated samples, microscopy techniques can help characterize the Hg-bearing species in complex multiphase natural samples.

Introduction

Mercury contamination of local, regional, and global environments has become an increasingly studied subject in recent years (*1–4*). Areas where Hg pollution has been most acute include abandoned Hg mines, gold mining areas where Hg was used in the amalgamation process, and industrial sites where Hg has been released as a byproduct of chemical processes (e.g., the electrochemical separation of chlorine from sodium salt at chlor-alkali plants). In all cases, knowledge of the molecular-level speciation of Hg is essential for understanding its potential bioavailability and impact on the environment. Determining the specific chemical forms of Hg present and their relative proportions in contaminated wastes has been particularly useful in establishing appropriate cleanup levels that protect humans or other biota in a cost-effective manner (*5*).

Methods for determining Hg speciation have increased in both number and sophistication over time, ranging from visual identification of Hg phases in ore-grade samples to sequential chemical extractions (SCE) (*6–8*), sequential thermal desorption (*9–11*), electron microprobe analysis (*12*), and in situ X-ray absorption spectroscopic analysis (*13*). Of these, sequential extractions have been most commonly used to determine Hg speciation, in part because of the ease, efficiency, and reproducibility of the procedure. SCE is a useful technique to provide information on the biogeochemically relevant fractionation of Hg present in sediments and soils (*6*) and features detection levels low enough (0.5 ng/g or ppb; *6*) to measure Hg in ambient sediments and soils. As with any single technique used for determining Hg speciation, however, inherent limitations exist. These include (i) the potential for transformation of Hg species during extraction; (ii) the nonspecific removal of Hg phases over multiple extraction steps; and (iii) the inconsistencies in speciation results between different extraction protocols (*14, 15*). As a result, SCE must define speciation operationally and thus may not yield accurate information in all cases on the Hg phases present in contaminated samples. Because of these limitations, it is useful to combine the sequential extraction method with other speciation and characterization techniques.

X-ray absorption fine structure (XAFS) spectroscopy has been shown to provide direct, in situ information on the speciation of heavy metal(loid)s such as arsenic, lead, and zinc in contaminated natural samples with minimal preparation or treatment prior to analysis (*16–22*). More recently, this technique has been used to identify the major Hg-containing phases and their relative proportions in contaminated samples with total Hg concentrations above 100 μg/g (ppm). The Hg XAFS analyses carried out to date (*13*) have shown that the Hg in Hg mine wastes is largely comprised of highly insoluble mercuric sulfides [cinnabar (HgS_{hex}) and metacinnabar (HgS_{cub})], with subordinate amounts of more soluble species such as mercuric chlorides, oxychlorides, and sulfates also present in some samples.

This study also demonstrated the relationship between Hg speciation in Hg mine wastes and the geological origin of the Hg ore. XAFS analyses of known mixtures of Hg-containing phases showed that the accuracy of the technique is of the order of 10% and that Hg-containing phases indicated by XAFS analysis at or below this percentage are not statistically significant (*13*). Limitations of the XAFS method include (i) the completeness of the Hg model compound database used in analysis (see Experimental Section); (ii) a concentration threshold of ~100 ppm, below which measurement of Hg L_{III} edge XAFS data is difficult using currently available synchrotron radiation sources and X-ray detectors; and (iii) the challenges in identifying Hg-containing phases in proportions too low to detect accurately (i.e., less than 10% currently) or of variable/poor crystallinity (e.g., elemental Hg).

The present study utilizes both XAFS spectroscopy and SCE to independently determine the Hg speciation of samples from a variety of Hg-contaminated environments. The two techniques are then compared to determine the consistency

* Corresponding author present address: Earth Sciences Division, Lawrence Berkeley National Laboratory, Bldg. 70R0108B, 1 Cyclotron Rd., Berkeley, CA 94720; e-mail: cskim@lbl.gov; phone: (510)486-7709; fax: (510)486-7152.
† Stanford University.
‡ Frontier Geosciences.
§ U.S. Geological Survey.
‖ Stanford Synchrotron Radiation Laboratory.

TABLE 1. Background Data for "Blind" Hg-bearing Samples Provided by Frontier Geosciences[a]

sample	description	[Hg]$_T$ (ppm)	location	matrix mineralogy
SFA	copper smelter fly ash	7539	El Paso, TX	anglesite, $PbSO_4$
MMS	mixed Hg standards in kaolinite	3490	synthetic	kaolinite, $Al_2Si_2O_5(OH)_4$
GMT1	gold mine tailings	635	Central California	deweylite, $(MgFe)_3(SiAl)_3O_7(OH)_4$
				quartz, SiO_2
GMT2	gold mine tailings	281	Central California	clinochrysotile, $Mg_3Si_2O_5(OH)_4$
				deweylite, $(MgFe)_3(SiAl)_3O_7(OH)_4$
				quartz, SiO_2
GMT3	gold mine tailings	140	Central California	baumite, $(MgMnFeZn)_3(SiAl)_2O_3$
				clinochrysotile, $Mg_3Si_2O_5(OH)_4$
				quartz, SiO_2
BTS	marine sediments	132	Bay of Trieste, Slovenia	calcite, $CaCO_3$

[a] Matrix mineralogy was determined later by XRD.

between results and explore any differences observed. Additional characterization methods including BET surface area analysis, X-ray diffraction (XRD), scanning electron microscopy (SEM), transmission electron microscopy (TEM), and energy-dispersive X-ray (EDX) spectrometry are applied to describe the bulk characteristics of each sample and to investigate both the sizes of Hg-bearing particles and the association of these particles with specific matrix phases.

Experimental Section

Six Hg-bearing samples, which were dry-sieved through either a 2.0- or a 1.4-mm sieve, were supplied as dry powders by Frontier Geosciences, Seattle, WA, for XAFS analysis. The total Hg concentrations of the samples ranged from 132 to 7539 ppm as determined by Frontier Geosciences by digestion in aqua regia (4:1 $HCl:HNO_3$) and analysis by cold vapor atomic fluorescence spectroscopy (CVAFS) using a modified version of U.S. EPA Method 1631 (23). No other information was provided regarding the samples prior to analysis by XAFS spectroscopy in order to ensure a "blind" study. Following XAFS analysis, background sample information (e.g., source location, sample type) was provided by Frontier Geosciences along with SCE results. Additionally, X-ray diffraction patterns were collected for each sample to identify the bulk mineralogy of the sample matrixes. This background sample information is shown in Table 1.

XAFS Analysis. XAFS analysis was conducted on all samples using the protocol reported in Kim et al. (13). Data were collected on wiggler-magnet beamlines 4-2 and 4-3 at the Stanford Synchrotron Radiation Laboratory (SSRL) using Si(111) and Si(220) monochromator crystals. Hg L_{III} edge XAFS spectra were collected on the samples as dry powders at room temperature in the fluorescence-yield mode using a 13-element, high-throughput germanium detector. This method is optimized for low-concentration samples (24). Arsenic and aluminum filters served to attenuate elastic scattering and background matrix fluorescence, respectively.

The speciation of Hg in the provided samples was determined by comparison of their XAFS spectra with those from a Hg model compound spectral database. Previously collected XAFS spectra of homogeneous, well-characterized crystalline and sorbed Hg phases comprise the database, shown in Figure 1. Phase and amplitude differences are evident among the 16 model spectra comprising the database; thus the individual spectra serve as unique "fingerprints" of component phases which can be identified in a heterogeneous Hg-bearing sample.

While a model compound spectrum represents the spectral fingerprint of a single pure Hg phase, the XAFS spectrum of a heterogeneous natural sample represents a sum of the XAFS contributions from all Hg phases present, weighted according to the atom percent of Hg in the sample
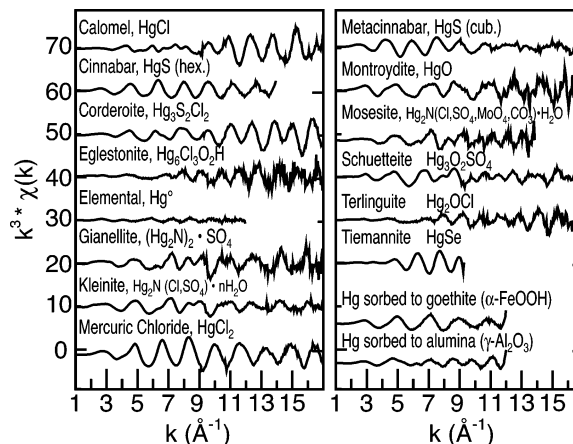
FIGURE 1. XAFS spectra of Hg minerals and Hg(II) sorption complexes in the model compound database used for linear least-squares fitting of the heterogeneous Hg-bearing samples. The horizontal axis represents the conversion of energy to momentum space following the normalization of the XAFS data to a fixed point in energy space. The vertical axis is a k^3-weighted expression of the XAFS function, which is modeled as the sum of scattering contributions from each neighboring shell of atoms.

and influenced by the degree of structural order around Hg in each sample. As such, the XAFS spectrum collected from a natural sample containing multiple Hg species can be decomposed using a linear least-squares fitting method into the sum of its individual components through direct comparison with the model compound spectra. Furthermore, determining the relative proportion of each model compound's contribution to the best possible linear combination fit allows quantification of the various phases present in the sample.

The linear least-squares fitting program DATFIT, a component of the data analysis package EXAFSPAK (25), was used to fit Hg L_{III} k^3-weighted XAFS spectra of natural samples with the XAFS spectra in the model compound database over a k range of 1–9 Å^{-1}. Single-component fits were first attempted in order to identify significant contributors (i.e., representing ≥10% of the overall spectrum) to the final fit. This subset of significant components was then used to generate two-component fits and so on, repeating the process until no more significant components could be identified or until the sum of all components reached 100% (±10%). An example of such a linear fit is shown in Figure 2, displaying fitting results for the SFA sample. The relative quality of the fit is indicated by the residual value, which represents the amount of the spectrum not accounted for by the linear fit and is calculated as a function of the difference between the
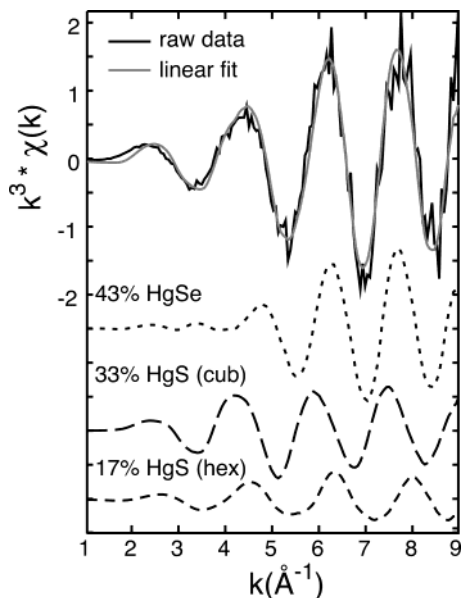
FIGURE 2. Linear fitting results for the SFA sample, showing the XAFS spectrum of the sample (black line), the best linear combination fit (gray line), and the components which contribute to the linear fit (dashed lines). In this case, the sample is found to consist of HgSe, metacinnabar, and cinnabar in proportions of 43%, 33%, and 17%, respectively, with a residual value of 0.076.

raw and the fitted values averaged over all points in the XAFS spectrum as follows:

$$\text{residual} = \frac{\sum_{i=1}^{n}(v_{\text{raw}} - v_{\text{fit}})^2}{n}$$

where v_{raw} is the value of raw data at a given point in k-space, v_{fit} is the value of linear least-squares fit at the same k value, and n is the total number of points in spectrum. Residual values may result from experimental noise, dilute samples yielding low-quality data, and/or incomplete fits in which an additional component was not included due to its absence from the model compound database.

To confirm the number of primary components present among the suite of samples analyzed, principal component analysis (PCA) was conducted using the data analysis program WinXAS (*26*) and the statistical software program Minitab. This procedure derives the number of components required to reconstruct a set of spectra within experimental error from the original spectra without use of model compound spectra (*27*). PCA therefore helps to constrain the results obtained from linear combination and standard fitting of either XAFS or X-ray absorption near-edge structure (XANES) spectra (*28–31*).

Sequential Chemical Extractions. SCE was conducted according to the protocol developed by Bloom et al. (*6*) based on the concept that exposure to increasingly powerful solvents will dissolve and extract Hg-containing species from a sample in a stepwise manner congruous with the relative solubilities of the Hg-containing phases present. Five extraction steps of increasing intensity (Table 2) were performed on the same set of samples analyzed by XAFS spectroscopy. A total of 0.4 g of solid was suspended in a 100:1 liquid-to-solid ratio and agitated constantly for 18 ± 3 h at 18–22 °C. Following centrifugation, the supernatant was filtered through a 0.2-μm filter. The extraction procedure was repeated on the sample pellet for 5–10 min as a rinse of the remaining solids, with the two filtrates combined and oxidized with

TABLE 2. Sequential Chemical Extraction Method for Determining Hg Speciation As Developed by Bloom et al. (*6*)[a]

step	extractant	description	typical compounds removed
F1	DI water	water soluble	$HgCl_2$
F2	pH 2 HCl/HOAc	"stomach acid"	HgO, $HgSO_4$
F3	1 N KOH	organocomplexed	Hg humics, Hg_2Cl_2, CH_3Hg
F4	12 N HNO_3	strong complexed	mineral lattice, Hg_2Cl_2, Hg^0
F5	aqua regia	mercury sulfides	HgS, HgSe

[a] Listed are the extraction steps, the general category of Hg-containing phases removed in each step, and specific Hg-containing compounds that are typically removed in that step.
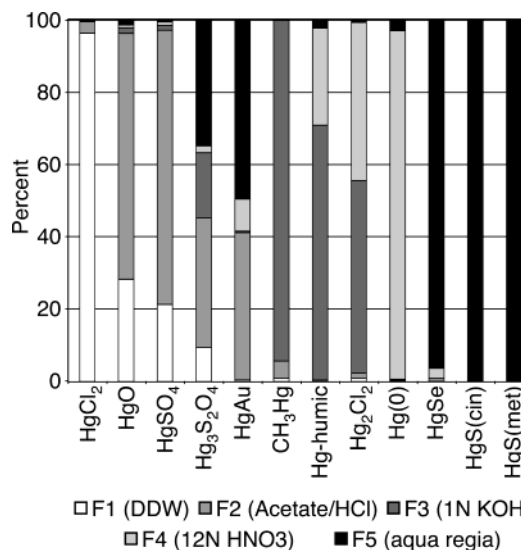
FIGURE 3. Sequential chemical extraction profiles for individual Hg compounds as developed by Bloom et al. (*6*).

BrCl prior to CVAFS analysis for dissolved Hg according to U.S. EPA Method 1631 (*23*). Error limits of this technique are estimated to be 5–10%, with method detection limits below 5 ppb for each specific extraction step.

The same extraction procedure was also conducted on several pure Hg-containing model compounds, which in most cases were diluted in an inert kaolinite matrix to achieve total Hg concentrations ranging from 1000 to 9600 ppm, thus avoiding saturation of the extracting solution (see ref *6* for more detail). This generated characteristic extraction profiles for the pure phases (Figure 3) and showed that while some Hg species are removed almost completely within one of the five extraction steps (e.g., $HgCl_2$, HgSe, HgS), others are extracted over multiple steps (e.g., $Hg_3S_2O_4$, $HgSO_4$, Hg_2Cl_2), demonstrating the nonspecificity of the SCE method mentioned earlier.

Additional Sample Characterization Techniques. Surface area measurements were conducted on all samples with a Coulter SA3100 surface area analyzer using the BET method (*32*). XRD spectra were collected using an XRD-1313 Rigaku Geigerflex diffractometer equipped with a Cu X-ray tube and graphite monochromator before the solid-state detector. Samples were step-scanned from 5 to 65° 2θ at angular increments of 0.05°, with 1.5 s counting time at each step. SEM and TEM analyses were conducted to characterize particle morphology, size, and surface characteristics. Additionally, EDX spectrometry was coupled with both SEM and TEM to identify or confirm the chemical composition of the sample matrixes as well as examine the association of Hg with specific matrix phases. TEM analyses were carried out at the National Center for Electron Microscopy at Lawrence Berkeley National Laboratories using a JEOL 200CX

Linear fit	Composition	Sum	Residual
SFA 7539 ppm Hg	43% Tiemannite, HgSe 33% Metacinnabar, HgS (cub) 17% Cinnabar, HgS (hex)	93%	0.076
MMS 3490 ppm Hg	48% Mercuric Chloride, $HgCl_2$ 32% Mercuric Oxide, HgO 27% Cinnabar, HgS (hex)	107%	0.075
GMT1 635 ppm Hg	60% Metacinnabar, HgS (cub) 31% Cinnabar, HgS (hex)	91%	0.063
GMT2 281 ppm Hg	49% Cinnabar, HgS (cub) 30% Metacinnabar, HgS (hex) 14% Schuetteite, $Hg_3O_2SO_4$	93%	0.060
GMT3 140 ppm Hg	64% Metacinnabar, HgS (cub) 28% Mercuric Oxide, HgO	92%	0.590
BTS 132 ppm Hg	62% Metacinnabar, HgS (cub) 38% Cinnabar, HgS (hex)	100%	0.196

FIGURE 4. Linear combination fits of the samples (black line = raw data, gray line = fit), raw quantitative compositional results, sums of components for each sample, and residual values corresponding to the quality of the fit.

scanning transmission electron microscope coupled with two Kevex X-ray detectors. SEM analyses were conducted on a JEOL JSM-5600 LV scanning electron microscope equipped with an EDX detector from EDAX, Inc.

Results and Discussion

XAFS/SCE. Results of XAFS analysis for all six samples are shown in Figure 4. Included are the XAFS spectra of the samples overlain by their best linear combination fits, the raw quantitative compositions of the Hg in each sample as determined by the linear fitting method, the summed percentage of all identified components, and the residual values associated with each fit. In all cases, the sum of the fitted components is between 91 and 107%, which is within the established degree of error for this technique and indicates that no significant components have been omitted. Table 3 compares the XAFS speciation results with those determined by SCE. The Hg species identified by XAFS spectroscopy have been listed next to the primary extraction steps demonstrated from earlier tests (Figure 3) to remove those particular species. Cinnabar and metacinnabar contributions have been consolidated in the XAFS results for simplicity, as the two polymorphs are both typically removed in the same extraction step (F5). An exception has been made in the case of sample BTS, where cinnabar and metacinnabar are listed separately to illustrate apparent differences in solubility.

The results of PCA using, as experimental spectra, the XAFS spectra generated from the samples and the model compounds identified in the linear combination fitting protocol (12 spectra total) indicate that a minimum of six components is required to reconstruct each of the experimental spectra in the set above a 95% confidence level. This analysis agrees with the linear fitting results, which determined that a set of six Hg-containing phases (HgS_{cub}, HgS_{hex}, HgSe, HgO, $HgCl_2$, and $Hg_3O_2SO_4$) was sufficient to define the speciation of each sample (Table 3, Figure 4). The PCA results serve as an independent check of the linear combination fitting process and imply that no significant Hg-containing phases are missing from either the model compound database or the final fits among the samples studied. A discussion of the speciation results for the individual samples as shown in Table 3 follows.

SFA. The identification of 50% mercury sulfides and 43% HgSe by XAFS spectroscopy matches well with the SCE results,

with 100% of available Hg removed in the F5 extraction which was shown (Figure 3) to remove mercury sulfides and HgSe. This comparison shows very good agreement between the two techniques, with XAFS spectroscopy providing quantitative information on the relative proportions of Hg phases present. Additionally, the high selenium concentration in this sample (6900 ppm) is consistent with the identification of HgSe in the sample by XAFS spectroscopy.

MMS. This sample was generated by mixing measured quantities of known Hg phases in a background matrix of kaolinite. XAFS analysis correctly identified the three Hg species ($HgCl_2$, HgO, and HgS (cinnabar)) present in the MMS sample. Additionally, the proportions of the phases as determined by XAFS spectroscopy (48%, 32%, and 27%, respectively) generally agree with those determined through SCE when adjusted for the nonspecific removal of HgO in the F1 and F2 extractions as shown in Figure 3 (35%, 26%, and 29%, respectively). However, both XAFS spectroscopy and SCE yield proportions of $HgCl_2$ and HgO that are contrary to their measured values of 18.2% and 45.2%, respectively, as shown in Table 4. The reason for this discrepancy is unknown but may indicate reactivity of the different Hg phases with one another and/or with the kaolinite matrix during the multistep extraction process. Such effects have been observed in extractions of other model compound mixtures (N. Bloom, personal communication) and have already been noted for single Hg phases (Figure 3), where nonspecific extraction of the phase over the course of several steps occurs due to reactivity and/or phase transformation during extraction.

GMT1. The identification of 91% mercury sulfides by XAFS spectroscopy agrees well with the removal of 93.1% Hg in the F5 extraction. The remaining 6.9% extractable Hg is distributed among the F1−F4 extractions. This level of agreement is within the experimental errors of both techniques.

GMT2. Schuetteite ($Hg_3S_2O_4$) and mercury sulfides represent 14% and 79%, respectively, of the Hg present according to XAFS spectroscopy. This corresponds well with the extraction results, in which 12.3% of the Hg is removed in the F4 extraction and 85.9% is removed in the F5 extraction. However, the model extraction profile for schuetteite shows a broad distribution of Hg removal over F1, F2, F3, and F5. This inconsistency between predicted and actual SCE results

TABLE 3. Comparison of Hg Speciation Results from XAFS and Sequential Chemical Extractions[a]

XAFS		extractions	
SFA: $[Hg]_T$ = 7539 ppm, SA = 6.4 m²/g			
		F1	0.0%
		F2	0.0%
		F3	0.0%
		F4	0.0%
mercury sulfides	50%	F5	100%
HgSe	43%		
[MMS: $Hg]_T$ = 3490 ppm, SA = 14.6 m2/g			
$HgCl_2$	48%	F1	46.2%
HgO	32%	F2	17.9%
		F3	0.5%
		F4	4.9%
mercury sulfides	27%	F5	29.1%
GMT1: $[Hg]_T$ = 635 ppm, SA=144.4 m²/g			
		F1	1.3%
		F2	1.2%
		F3	1.0%
		F4	3.4%
mercury sulfides	91%	F5	93.1%
GMT2: $[Hg]_T$ = 281 ppm, SA = 88.9 m²/g			
		F1	0.4%
schuetteite	14%	F2	0.8%
		F3	0.5%
		F4	12.3%
mercury sulfides	79%	F5	85.9%
GMT3: $[Hg]_T$ = 140 ppm, SA = 49.3 m²/g			
		F1	7.0%
mercuric oxide	28%	F2	0.0%
		F3	0.0%
		F4	23.1%
mercury sulfides	64%	F5	69.9%
BTS: $[Hg]_T$ = 132 ppm, SA = 5.6 m²/g			
		F1	0.0%
		F2	0.0%
		F3	1.0%
		F4	68.6%
metacinnabar	62%	F5	30.4%
cinnabar	38%		

[a] Total Hg concentrations and measured BET surface areas are also included. Hg-containing phases identified by XAFS spectroscopy are listed adjacent to the extraction steps anticipated (based on Figure 3) to remove those particular species.

may be due to factors such as encapsulation of the schuetteite within larger particles, which would inhibit Hg removal until later extractions, or a misidentification of the non-mercury sulfide phase; in the latter case, schuetteite may provide the best fit among the model compound spectra available, when in fact a different Hg phase is present that bears spectral similarities to schuetteite but features a different extraction profile.

GMT3. The characterization of 64% mercury sulfides by XAFS spectroscopy matches closely with the 69.9% Hg removed in the F5 extraction. The remaining extractable Hg is removed primarily during the F4 extraction (23.1%); however, XAFS spectroscopy identifies the 28% of Hg present as HgO, which should be removed in the F1 and F2 extractions according to its model extraction profile. This is a similar problem as observed in the previous sample and is subject to the same potential explanations for the discrepancy. Additionally the high level of experimental noise in this sample, reflected in its large residual, makes XAFS characterization of the secondary Hg phase in this sample uncertain.

BTS. XAFS spectroscopy indicates that the Hg in this sample consists entirely of mercury sulfides (100%). Sequential extractions, however, show that 68.6% of the extractable Hg is removed in the F4 extraction, which should

not be sufficient to remove mercury sulfides. Differentiating between the two mercury sulfide polymorphs however shows that the Hg removed in the F4 and F5 extractions (68.6% and 30.4%, respectively) appears to correspond with the proportions of metacinnabar and cinnabar present (61% and 39%). This indicates that the proportion of Hg identified by XAFS as metacinnabar is more soluble in this natural sample than would be predicted from model extraction tests and is removed in the F4 extraction instead. Potential explanations for such a difference in metacinnabar extractability include elevated amounts of impurities such as Fe and Zn, which are common in natural metacinnabar (*33*) and can affect physical and chemical characteristics such as its solubility and the inversion temperature between cinnabar and metacinnabar (*34*). Also, the inverse relationship between particle size and extraction efficiency, which has been documented in CuS and NiS model systems (*35*), may result in enhanced Hg removal during earlier extraction steps. Particularly at relatively low total amounts of Hg (<100 μg), the proportion of mercury sulfides removed by less stringent solvents such as concentrated HCl can increase significantly (*36*). Such factors may be particularly enhanced in reducing natural systems where nanoparticulate metacinnabar can form (*12*).

Additional Sample Characterization Techniques. Table 1 contains the results of the XRD studies conducted following XAFS analysis. Notably, no Hg-bearing phases are detectable by XRD, as they represent a very minor proportion of the crystalline phases in the samples (mineral phases must typically be present in the several percent range in order to be detected by XRD). Sample surface areas are included in Table 3 and, among the GMT samples, show a strong positive correlation between surface area (which is often a proxy for particle size), total Hg concentration, and the proportion of Hg-sulfides present as determined by both XAFS and sequential extractions. This observation is consistent with the low hardness values of cinnabar and metacinnabar (2.5 and 3, respectively; *37*), which can result in more rapid physical weathering of these Hg phases relative to other harder matrix minerals. Such preferential weathering could lead to a progressive enrichment of both insoluble mercury sulfides and total Hg concentrations in the smaller particle size fractions, with soluble Hg phases likely to dissolve more rapidly due to the increased reactive surface areas. This process corresponds with the studies of Harsh and Doner (*38*) and Nelson et al. (*39*), who have observed elevated concentrations of mercury sulfides in very fine sand and silt fractions relative to larger grain size fractions in northern California and Alaska, respectively. Our own studies with size-fractionated mine waste samples confirm that this trend is more common than previously thought (*40*).

TEM and SEM images along with EDX spectra of individual particles were collected to determine particle morphology, average particle size and size range, chemical information for specific phases, and, where possible, association of Hg with bulk matrix phases. Hg species were identified in the two most highly concentrated samples, SFA (7539 ppm Hg) and MMS (3490 ppm Hg). SEM images and corresponding EDX analysis of MMS (not shown) reveal that Hg is present as discrete particles of the phases identified by XAFS spectroscopy ($HgCl_2$, HgO, HgS) dispersed indiscriminately in a matrix of kaolinite particles, which is consistent with the manner in which the sample was generated. In contrast, the Hg present in SFA appears to be affiliated primarily with an amorphous Si/K-bearing phase (undetected by XRD) and not the particles of anglesite ($PbSO_4$), which constitute the dominant crystalline phase in the sample. Specifically, TEM and EDX analyses show that Hg is present as nanocrystalline ($\sim$50 nm) HgS and HgSe particles enmeshed in the amorphous matrix phase (Figure 5). This is consistent with both XAFS and SCE results and provides additional information

TABLE 4. Comparison of the Known Hg Speciation of Sample MMS with Speciation As Determined by XAFS and Sequential Chemical Extractions[a]

phase	known speciation (%)	XAFS (%)	extractions (%)	extractions (adjusted)	extractant
$HgCl_2$	18.2%	48%	46.2% (F1)	35% $HgCl_2$	water (removes $HgCl_2$)
HgO	45.2%	32%	17.9% (F2)	26% HgO	1 N HCl (removes HgO)
			0.5% (F3)		1 N KOH
			4.9% (F4)		12 N HNO_3
HgS, cin.	36.6%	27%	29.1% (F5)	29% HgS, cin	aqua regia (removes HgS)

[a] The sequential extraction results have been adjusted for the nonspecific extraction profile of HgO (Figure 3) to calculate the abundances of these phases in the sample based on the extractions.
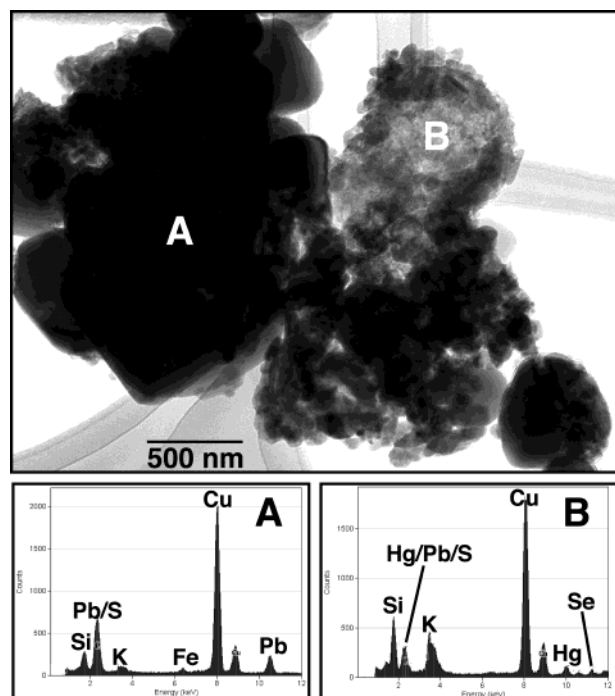
FIGURE 5. TEM image of sample SFA, showing the particles of anglesite ($PbSO_4$) and an amorphous Si-bearing phase that was undetectable by XRD due to its poor crystallinity (Cu peak arises from the sample grid). The EDX spectra (below the image) show that Hg is associated with the amorphous Si-containing phase and not with the anglesite grains.

regarding particle size and matrix phase affiliation. The enhanced transport potential of Hg in the colloidal phase (*41, 42*) underscores the importance of generating such complementary information through microscopy techniques.

Assessment of the XAFS/SCE Comparison. In nearly all samples examined, the proportion of mercury sulfides (and HgSe for sample SFA) identified by XAFS spectroscopy corresponds very well with the proportion of Hg removed in the F5 extraction within the estimated experimental error of ~10%. This finding is consistent with the fact that aqua regia, the F5 extractant, is typically the only solvent capable of dissolving highly insoluble mercury sulfide and HgSe species as documented in the model extraction profiles (Figure 3). The good agreement between the two techniques in this regard applies over the wide range of Hg concentrations and sample types examined in this study. One exception is the BTS sample, where a substantial proportion of the Hg present was removed in the F4 fraction despite the identification of only cinnabar and metacinnabar in the sample by XAFS spectroscopy; as mentioned before, this may be due to impurity or particle size effects in the metacinnabar that increase its apparent solubility.

Differences in Hg speciation determined by the two techniques arise when characterizing the more soluble non-mercury sulfide fraction, where Hg-containing phases identified by XAFS spectroscopy are removed in extraction steps different from those predicted based on model extraction profiles. These inconsistencies could occur for several reasons, many of which involve the morphology and association of Hg with other matrix phases in the sample. These include (i) encapsulation effects in which Hg-containing phases are enclosed within larger, less soluble particles; (ii) variable crystallinity of a phase, with less crystalline phases being more soluble than more crystalline phases; (iii) particle size/surface area effects, with nanometer-sized particles being more soluble than larger particles of the same phase; and (iv) direct chemical association or reactivity of Hg-containing phases with the mineral matrix induced during the extraction process. Such effects have the potential to influence the relative solubility of specific phases during SCE and/or the accurate identification of the Hg-containing phases present.

The above reasons for differences in Hg speciation results between XAFS spectroscopy and sequential extractions are likely to be even more pronounced at lower total Hg concentrations. As the amount of Hg available for XAFS analysis or SCE decreases in a sample, the relative errors and potential interferences are expected to increase. This is evidenced by higher residual values during XAFS spectral fitting and more significant deviations between results of the two techniques.

In cases where quantitative differences are evident between the XAFS and the selective extraction results, additional characterization using techniques such as BET surface area analysis, SEM, TEM, and XRD can provide potentially useful information on the matrix mineralogy, particle morphology and size, and interaction of phases in the sample of interest. At high total Hg concentrations (≥ 1000 ppm), where Hg-containing phases can be directly detected with electron microscopy, SEM and TEM can also provide information on the morphology and association of the Hg-containing phases within the sample matrix. The use of multiple analytical methods, including the newer technique of XAFS spectroscopy, to define Hg speciation in mine wastes and contaminated soils and sediments is highly recommended in order to improve predictions of the potential availability of Hg and to develop effective remediation strategies.

Acknowledgments

Literature Cited

(1) Davis, A.; Bloom, N. S.; Que Hee, S. S. *Risk Anal.* **1997**, *17*, 557−569.

(2) Jackson, T. A. *Environ. Rev.* **1997**, *5*, 99−120.

(3) Wolfe, M. F.; Schwarzbach, S.; Sulaiman, R. A. *Environ. Toxicol. Chem.* **1998**, *17*, 146−160.

(4) Schluter, K. *Environ. Geol.* **2000**, *39*, 249−271.

(5) U.S. EPA. Environmental Protection Agency Report EPA-505-D-96-001; 1996; 4 pp.

(6) Bloom, N. S.; Pereus, E.; Katon, J.; Hiltner, M. *Anal. Chim. Acta* **2003**, *479*, 233−248.

(7) Sakamoto, H. T.; Tomiyasu, T.; Yonehara, N. *Anal. Sci.* **1992**, *8*, 35−39.

(8) Revis, N. W.; Osborne, T. R.; Holdsworth, G.; Hadden, C. *Water, Air, Soil Pollut.* **1989**, *45*, 105−113.

(9) Biester, H.; Gosar, M.; Covelli, S. *Environ. Sci. Technol.* **2000**, *34*, 3330−3336.

(10) Biester, H. *J. Geochem. Explor.* **1999**, *65*, 195−204.

(11) Biester, H.; Scholz, C. *Environ. Sci. Technol.* **1997**, *31*, 233−239.

(12) Barnett, M. O.; Harris, L. A.; Turner, R. R.; Stevenson, R. J.; Henson, T. J.; Melton, R. C.; Hoffman, D. P. *Environ. Sci. Technol.* **1997**, *31*, 3037−3043.

(13) Kim, C. S.; Brown, G. E., Jr.; Rytuba, J. J. *Sci. Total Environ.* **2000**, *261*, 157−168.

(14) Martin, J. M.; Nirel, P.; Thomas, A. J. *Mar. Chem.* **1987**, *22*, 313−341.

(15) Barnett, M. O.; Harris, L. A.; Turner, R. R.; Henson, T. J.; Melton, R. E.; Stevenson, R. J. *Water, Air, Soil Pollut.* **1995**, *80*, 1105−1108.

(16) Morin, G.; Ostergren, J. D.; Juillot, F.; Ildefonse, P.; Calas, G.; Brown, G. E., Jr. *Am. Mineral.* **1999**, *84*, 420−434.

(17) Ostergren, J. D.; Brown, G. E., Jr.; Parks, G. A.; Tingle, T. N. *Environ. Sci. Technol.* **1999**, *33*, 1627−1636.

(18) Foster, A. L.; Brown, G. E., Jr.; Tingle, T.; Parks, G. A. *Am. Mineral.* **1998**, *83*, 553−568.

(19) Hesterberg, D.; Savers, D. E.; Zhou, W.; Plummer, G. M.; Robarg, W. P. *Environ. Sci. Technol.* **1997**, *31*, 2840−2846.

(20) Manceau, A.; Boisset, M. C.; Sarret, G.; Hazemann, J. L.; Mench, M.; Cambier, P.; Prost, R. *Environ. Sci. Technol.* **1996**, *30*, 1540−1552.

(21) Cotter-Howells, J. D.; Champness, P. E.; Charnock, J. M.; Pattrick, R. A. D. *Eur. J. Soil. Sci.* **1994**, *45*, 393−402.

(22) Scheinost, A. C.; Kretzschmar, R. S.; Pfister, S.; Roberts, D. R. *Environ. Sci. Technol.* **2002**, *36*, 5021−5028.

(23) U.S. EPA. Environmental Protection Agency Report EPA-821-R-01-024; 2001; 36 pp.

(24) Waychunas, G. A.; Brown, G. E., Jr. *Adv. X-Ray Anal.* **1994**, *37*, 607−617.

(25) George, G. N.; Pickering, I. J. Stanford Synchrotron Radiation Laboratory report. 1995; 63 pp.

(26) Ressler, T. *J. Synchrotron Radiat.* **1998**, *5*, 118−122.

(27) Malinowski, E. R. *Factor analysis in chemistry*, 2nd ed.; Wiley & Sons: New York, 1991.

(28) Ressler, T.; Wong, J.; Roos, J.; Smith, I. L. *Environ. Sci. Technol.* **2000**, *34*, 950−958.

(29) Wasserman, S. R. *J. Phys. IV* **1997**, *7*, 203−205.

(30) Wasserman, S. R.; Allen, P. G.; Shuh, D. K.; Bucher, J. J.; Edelstein, N. M. *J. Synchrotron Radiat.* **1999**, *6*, 284−286.

(31) Beauchemin, S.; Hesterberg, D.; Beauchemin, M. *Soil Sci. Soc. Am. J.* **2002**, *66*, 83−91.

(32) Brunauer, S.; Emmett, P. H.; Teller, E. *J. Am. Chem. Soc.* **1938**, *60*, 309−319.

(33) Tauson, V. L.; Akimov, V. V. *Geochim. Cosmochim. Acta* **1997**, *61*, 4935−4943.

(34) Dickson, F. W.; Tunell, G. *Am. Mineral.* **1959**, *44*, 471−487.

(35) Cooper, D. C.; Morse, J. W. *Environ. Sci. Technol.* **1998**, *32*, 1076−1078.

(36) Mikac, N.; Foucher, D.; Niessen, S.; Fischer, J.-C. *Anal. Bioanal. Chem.* **2002**, *374*, 1028−1033.

(37) Klein, C.; Hurlbut, C. S., Jr. *Manual of Mineralogy*, 20th ed.; John Wiley & Sons: New York, 1985.

(38) Harsh, J. B.; Doner, H. E. *J. Environ. Qual.* **1981**, *10*, 333−337.

(39) Nelson, H.; Larsen, B. R.; Jenne, E. A.; Sorg, D. H. *Science* **1977**, *198*, 820−824.

(40) Kim, C. S.; Rytuba, J. J.; Brown, G. E., Jr. *Appl. Geochem.* (in press).

(41) Babiarz, C. L.; Hurley, J. P.; Hoffmann, S. R.; Andren, A. W.; Shafer, M. M.; Armstrong, D. E. *Environ. Sci. Technol.* **2001**, *35*, 4773−4782.

(42) Roth, D. A.; Taylor, H. E.; Domagalski, J.; Dileanis, P.; Peart, D. B.; Antweiler, R. C.; Alpers, C. N. *Arch. Environ. Contam. Toxicol.* **2001**, *40*, 161−172.